minerals

MDPI

Article

Properties of Bentonite-Based Sealing Materials during Hydration

Mahsa Shafaei Bajestani, Othman Nasir * and Won Taek Oh

Department of Civil Engineering, University of New Brunswick, Fredericton, NB E3B 5A3, Canada; mahsa.shafaei@unb.ca (M.S.B.); woh@unb.ca (W.T.O.)
* Correspondence: othman.nasir@unb.ca; Tel.: +1-506-453-4914

Abstract: A typical deep geological repository (DGR) design consists of a multi-barrier system, including the natural host rock and the engineered barrier system. Understanding the swelling behavior of bentonite-based sealing materials (BBSM), as a candidate material for the engineered barrier system, is crucial for DGR's long-term safety. In this study, a hydromechanical (HM) column-type test was designed to model the hydration of BBSM from the underground water and determine the resulting swelling pressure in vertical and radial directions. Five hydration tests were carried out on identical compacted samples of 70% bentonite and 30% sand (70-30 bentonite-sand) mixtures with a dry density of 1.65 g/cm^3 for varied durations of hydration, between 1 day and 120 days. The experiments were performed parallel to the compaction direction. Following each HM column-type test, the advancement of the wetting front was determined for each test. After 120 days, 56,339 mm^3 of water infiltrated the sample and the wetting front reached over 50% of the sample height. The evolution of axial swelling pressure revealed an initial increase in swelling pressure with time in all tests, followed by a reduction in the rate at later times. After early stages of swelling, radial sensors showed an increase in swelling pressure. After 120 days, the radial pressure sensor closest to the hydration front showed 52% more radial pressure than the axial swelling pressure.

Keywords: deep geological repository; bentonite-based sealing materials; engineered barrier systems; hydromechanical process; column-type test; swelling pressure

Citation: Bajestani, M.S.; Nasir, O.; Oh, W.T. Properties of Bentonite-Based Sealing Materials during Hydration. *Minerals* **2023**, *13*, 1412. https://doi.org/10.3390/min13111412

Academic Editors: Ana María Fernández, Thanh Son Nguyen and Mamadou Fall

Received: 30 August 2023
Revised: 29 October 2023
Accepted: 2 November 2023
Published: 4 November 2023

1. Introduction

The majority of nuclear management organizations selected the concept of the deep geological repository (DGR) as a preferred method for the disposal of radioactive wastes [1–4]. The safety of the DGR relies on a multi-barrier system, which mainly consists of the natural geological barrier, (i.e., the host rock and the engineered barrier system), to isolate the radioactive wastes from the living biosphere [5]. Figure 1 presents the simplified illustration of the DGR concept proposed by NWMO (Nuclear Waste Management Organization, Canada), known as Mark II [2,6]. The DGR is constructed at a depth of several hundred meters below the ground surface in a host rock formation and includes a network of surface facilities, access tunnels, ventilation shafts, and placement rooms for used fuel containers (UFC). Different nuclear waste organizations have investigated a variety of geological formations as a host rock formation, such as sedimentary rock (like shale and clay formation), crystalline rocks (like granite), and salt formations (like salt domes or bedded salt) [2–5].

Along with the host rock barrier the engineered barrier system includes different components, such as backfill materials and containers, to ensure the safety of the DGR system. Compacted bentonite-based sealing materials (BBSM) are essential elements of the engineered barrier system of DGR because of their low permeability, high swelling potential, and retention of radionuclides. Various concepts could be used in designing the DGR system, depending on different factors such as the host rock formation and the types of BBSM and UFC in placement rooms. For instance, in the DGR concept of NWMO

(Mark II), as shown in Figure 1, each UFC will be encased in the compacted BBSM block and separated from the next block with compacted BBSM spacer blocks, and bentonite pellets materials, as dense backfill, will be used to fill the technological voids of placement rooms [2,6].

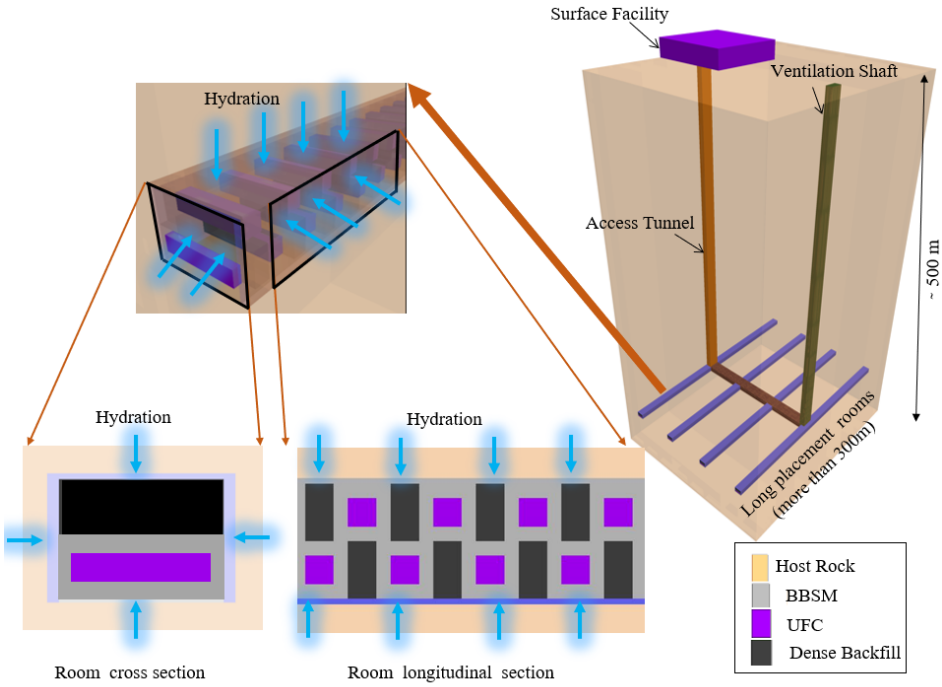

Figure 1. Simplified illustration of NWMO DGR concept (Mark II) (for demonstration, not to scale) [2,6].

Following the placement of the unsaturated BBSM and the closure of the DGR, the groundwater is expected to infiltrate the materials from the host rock, followed by the hydration process and swelling of clay minerals [7]. Swelling of clay minerals is the change in volume resulting from changes in water content under mechanically constrained conditions; when the increase in volume is limited, then the swelling processes will result in an increase in the confining pressure until it reaches a maximum value, known as the swelling pressure [8]. According to Mitchell and Soga [9], one reason for the swelling process of BBSM could be due to the hydration of interlayer cations and an increase in ion volume, in the case of cation exchange, followed by an increase in soil volume. This volume change during the interlayer hydration is referred to as crystalline swelling [10]. Another reason for the swelling process is that water is absorbed by hydrogen bonding to the surface of clay particles, leading to a significant surface hydration energy that overcomes the van der Waals forces existing between the layers, a process which thereby contributes to an increased volume of the soil [9]. The surface hydration also plays a role in the volume changes because of the diffuse double layer (DDL), a zone where ions are not strongly attracted to the surface and able to move more freely and therefore can cause particles or layers to be pushed further apart [10].

Nasir et al. [11] introduced a multi-scale porosities concept defining micro-porosity (the intra-element porosity or the porosity between each clay grain), macro-porosity (the porosity between clay aggregates and other materials in the mixture such as sand), mega-porosity (the void between bentonite pellets), and gap-porosity (the space between the BBSM and rock or other structures). Nasir et al. [11] also proposed that there are three swelling states: preliminary, advanced, and full swelling. When water infiltrates into unsaturated BBSM, the preliminary swelling takes place because of chemical bonding between water molecules and clay particles within the intra-elements. In the preliminary swelling, the clay surface, which carries a negative charge, will attract a positively charged

end of water molecule that results in the formation of a strongly attracted layer of water. During the preliminary state, the swelling will work to increase micro-porosity, while decreasing all other porosities. At this state the permeability of the BBSM is dominated by the high macro-porosity, leading to a high total permeability and faster water infiltration. Following this state, the advanced swelling state will start, and the swelling intra-elements will lead to a decrease in macro-porosity, occupied by swelling intra-elements, and hence—a decrease in total permeability. This mechanism of changes in pore size distribution was observed experimentally by Seiphoori et al. [12], whose results showed a reduction in macro-porosity and an increase in micro-porosity following the wetting process. This process can be conceptualized as changing the BBSM structure from a coarse grain to fine materials. The advanced swelling state begins when the surface of clay particles is covered by a strongly attracted layer of water. At the advanced swelling state, the BBSM is still unsaturated, and the clay particles continue to attract additional water to form the DDL. In this state, properties of BBSM, such as permeability, are evolving and can vary depending on different variables such as saturation and confining stress. BBSM will adsorb water, resulting in an increase in volume under free swelling conditions and an increase in swelling pressure under confined conditions. In the full-swelling state the BBSM reaches the zero swelling potential, the swelling process is completed, and the materials' properties will not change [11]. Complete saturation may require hundreds to thousands of years based on the availability and pressure of water supply and the permeability of the host rock and BBSM [13,14].

Re-hydration of BBSM could cause bentonite to swell and fill voids and gaps in the DGR system. After filling the gaps, a swelling pressure will develop in both the radial and axial directions under constant-volume conditions. The evolution of swelling pressure, volume change, and the rate of saturation change are all of the potential interactions between the host rock and BBSM as an engineered barrier system that should be taken into account during the design of the DGR system in order to maintain overall stability. The swelling pressure should be high enough to support long-term sealing properties. Most of the safety assessment scenarios count on the multi-barrier system, including UFC, BBSM, and the natural host rock. In case of a potential scenario where both UFC and BBSM fail to contain the radioactive materials, the main barrier will be the host rock. In this case, the swelling pressure should not exceed the in situ minor principal stress to avoid hydrofracturing of the rock formations and ensure its barrier performance [2]. Hence, the investigation of the swelling properties of BBSM during the re-hydration process is crucial to assess the safety of the whole DGR.

Many contributions are made to understanding the HM behavior of hydrated bentonite, using a wide range of full-scale experiments in underground research laboratories (URL). Examples include the Tunnel Sealing Experiment (TSX) at Manitoba, Canada [15]; the Full-Scale Engineered Barriers Experiment (FEBEX) at Grimsel, Switzerland [16]; RESEAL at Mol, Belgium [17,18]; and the Engineered Barriers (EB) test at the Mont Terri URL [19]. These experiments have provided data to evaluate the response of the multi-barrier system of the DGR, improving the conceptual understanding of coupled processes affecting bentonite behavior and allowing the development of numerical models [20]. In parallel to the full-scale testing, several mock-up tests have been performed on the hydration process of BBSM. For example, the SEALEX experiment was performed by IRSN (Institut de Radioprotection et de Sûreté Nucléaire, France) in the Tournemire underground research laboratories (URL) as part of the DECOVALEX project to investigate the major factors related to the hydromechanical (HM) behavior of bentonite materials [21]. The SEALEX experiments were carried out on a compacted mixture of 70% MX80 bentonite and 30% sand, with dry densities between 1.67 and 1.97 g/cm^3 [21]. Before starting the in situ test of the SEALEX experiments, a mock-up test, which was 1/10th of the size of the in situ experiment, was performed in controlled laboratory conditions to provide information about saturation time and sealing properties of the materials [21]. The in situ test of the SEALEX project included the injection of synthetic water, which had the same

chemical composition as the water within the host rock of the Tournemire URL, through bentonite materials installed into a 60 cm diameter horizontal borehole excavated in the host rock. The in situ test of the SEALEX project measures the axial and radial stresses and relative humidity at different sample locations [21]. Modeling of laboratory mock-up and in situ experiments of the SEALEX project was performed by applying different conceptual models, codes, and software such as COMSOL, CODE_BRIGHT, QPac, and OGS; the results of different modeling teams were compared with the experimental data. Comparing the experimental data of swelling pressure with different proposed numerical formulations was utilized to predict the HM behavior and characteristics of BBSM. The numerical studies of the mock-up and in situ experiments of the SEALEX project, in general, performed well and could often predict the endpoints of the experiment, such as swelling pressure and the amount of injected water. The details of the transient effects, however, were much more difficult to predict [13,20,22–24].

The mock-up laboratory tests have several benefits over full-scale experiments, such as a lower cost of conducting the test, a reasonable testing period, control of the boundary and initial conditions, and the efficiency of data monitoring [25,26]. The column-type test can be used to study HM behaviors of BBSM, such as the changes in hydraulic properties and the evolution of the swelling pressure with time. A series of reduced-scale mock-up tests were carried out using column-type testing devices to investigate the response of several coupled processes in bentonite materials by tracking temperature, saturation distribution, and swelling pressure development [21,25,27–34]. For instance Cui et al. [34] carried out three infiltration tests under constant-volume conditions and one test under the free swell condition on Kunigel-V1 bentonite–sand mixture samples in a cylindrical metallic cell with a 50 mm diameter and 250 mm height. The cell was equipped with humidity sensors to determine the hydraulic conductivity of unsaturated materials. Schanz et al. [25] designed a column device that applied temperature and hydraulic gradients from both sides of the column on a mixture of sand and Calcigel bentonite. Schanz et al. [25] focused on measuring swelling pressure only on the top and bottom of the sample under temperature and hydraulic loading. Most of the mentioned investigations that used the column-type experiments have not considered the axial and radial swelling pressure measurements during the hydration of bentonite materials in the column-type device.

The swelling pressure developed during the hydration process is dependent on the rate of saturation and the stiffness of the boundary (restraint), which can vary in both the axial and radial directions [26]. Saba et al. [35] conducted two small-scale mock-up tests with 60 mm diameter and 118 mm height cylinders under constant-volume conditions. The first test was subjected to saturated boundary conditions from the bottom only, while the second test was subjected to saturated boundary conditions from both the bottom and top. Based on the study of Saba et al. [35], the axial and radial swelling pressure measured at different positions showed the anisotropic swelling behavior of bentonite materials and the relation of radial swelling pressure to the distance from the hydration end. To investigate the suction changes during the hydration, Saba et al. [35] discussed the results of swelling pressure based on the hydraulic parameters of the SEALEX mock-up test on the same mixture of 70% MX80 bentonite and 30% sand, which were also investigated by Wang et al. [36] in a separated study. Most of the previous studies were focused on axial swelling pressure and saturated hydraulic conductivity. By considering different column-type tests of coupled processes, a few investigations have focused on determining the axial and radial stress and the measurement of the hydration properties at the same time in column-type testing [26,37]. Rawat et al. [26] performed a water infiltration test on the compacted Calcigel bentonite–sand mixture (50:50) to study the material response under hydraulic gradient due to the hydration of the mixture. Rawat et al. [26] analyzed the measured axial and radial stresses, which demonstrated a higher swelling pressure in the radial direction along the sample than in the axial direction. According to the findings of Rawat et al. [26], the axial stress reached 1.68 MPa in 349 days, whereas the radial swelling pressure reached higher than 2 MPa within the same time. Liu et al. [37]

conducted the infiltration test on a GMZ bentonite pellet mixture with a dry density of 1.45 g/cm^3 in a stainless steel cell with 5 cm diameter and 15 cm height to evaluate the hydromechanical response by measuring the humidity and swelling pressure. Based on the study of Liu et al. [37], the axial swelling pressure evolved smoothly with a peak of 0.5 MPa, while radial swelling pressure evolved at different trends, with a peak of 1.5 MPa recorded by the sensor close to the hydration front.

The focus of this study is on the experimental investigation of the hydromechanical process (HM) of compacted bentonite materials during hydration. A better understanding of the coupled HM behavior of bentonite materials can be obtained by determining the axial and radial stress and the measurement of the water flow rate and advance in water saturation front. This study investigated the HM behavior of bentonite materials using a new HM column-type test with a modified triaxial device setup to mimic the in situ process, measure the swelling pressures, and determine the actual water saturation by extracting slices at a certain location along the height of the sample.

2. Materials and Methods

2.1. Materials

In this study, a mixture of 70-30 bentonite-sand was used to investigate the effect of the hydration process on the swelling pressure. The materials used are shown in Figure 2.

(**a**) (**b**)

Figure 2. Materials used in this study: (**a**) bentonite; (**b**) sand.

Commercial sodium bentonite from Lovell Wyoming bentonite plants [38] was used. This bentonite contains mainly swelling smectites, a smaller fraction of non-swelling minerals, and an initial water content of 10% [38]. The elemental analysis, by X-ray Fluorescence and X-ray diffraction, of the aforementioned bentonite was carried out by The Mineral Lab Inc., Golden, CO, USA [38]. The elemental analysis results showed the used bentonite chemical compositions, which are presented in Table 1.

Table 1. Chemical composition of bentonite used.

Chemical Compositions	Value
SiO_2	59.9%
Al_2O_3	17.6%
CaO	2.64%
Na_2O	2.51%
MgO	1.83%
Fe_2O_3	3.72%
K_2O	0.6%
MnO_2	0.08%

The analysis of X-ray diffraction demonstrated the primary mineral components of bentonite as follows: montmorillonite (75%), illite (5%), feldspar (less than 3%), and quartz (less than 3%) [38]. Based on the Atterberg limit tests, the liquid limit of this bentonite is 493%, and its plasticity index is 452%. The cation exchange capacity (CEC) was determined to be 75 meq/100 g by performing the methylene blue test using the procedure of ASTM Standard C 837-09 [39]. The free swelling index test [40] was performed to identify the swelling potential of the bentonite material used in the present study, which showed an average differential free swelling index of 1578.5%. Figure 3 shows the particle size distribution of bentonite, as measured by hydrometer analysis. The grain size distribution shows that 67% of the grains are smaller than 2 µm (clay fraction).

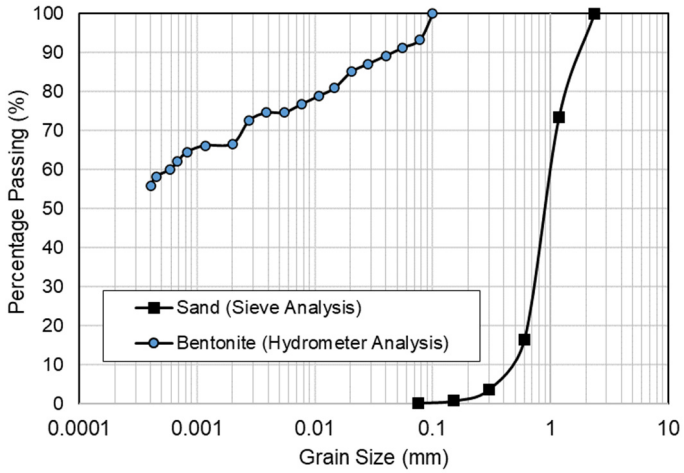

Figure 3. Grain size distribution of bentonite and sand.

The sand used was Silica white sand, also known as quartz sand [41]. According to the sieve analysis of the sand shown in Figure 3, the uniformity coefficient (C_u) and the coefficient of curvature (C_c) were determined to be 2 and 1.1, respectively, indicating poorly graded sand (SP).

In this study, the water retention curve (WRC) of the bentonite–sand mixture was determined by combining saturation–suction points from the vapor equilibrium technique and the chilled mirror technique. The saturated salt solutions used for the vapor equilibrium technique, which included potassium carbonate (K_2CO_3), sodium chloride (NaCl), and polyethylene glycol (PEG), were selected to have points with low, medium, and high suction. Table 2 shows the corresponding suction to each salt solution. Three identical compacted samples with 50 mm diameter and 20 mm height were used for each salt solution. WP4C device (METER Group Inc., Pullman, WA, USA) was used to measure the suction based on the chilled mirror method [42]. The compacted mixture in the cup was set in the sample drawer of the device, and the drawer was closed and sealed. The instrument determines the relative humidity using the chilled mirror method once the sample comes into equilibrium with the vapor in the sealed chamber. Nineteen samples with different degrees of saturation were tested in WP4C and each test was repeated two times.

Table 2. Saturated salt solutions.

Saturated Salt Solution	Suction (MPa)
PEG	0.1
NaCl	38
K_2CO_3	113

A fitted WRC curve was generated using the van Genuchten [43] equation:

$$s = -(1/\alpha)(S_{ec}{}^{-1/m} - 1)^{1/n}$$
$$S_{ec} = (S_l - S_{lr})/(1 - S_{lr}) \quad (1)$$

where s is suction (MPa); S_{ec} is effective saturation; S_l is liquid saturation; S_{lr} is residual liquid saturation; a, m, and n are fitting parameters of van Genuchten's model.

Figure 4 shows the WRC of the mixture and fitted curve. The R-squared fitting of the WRC curve was 0.93. Table 3 gives a summary of the basic properties of the materials and WRC fitting parameters of the mixture.

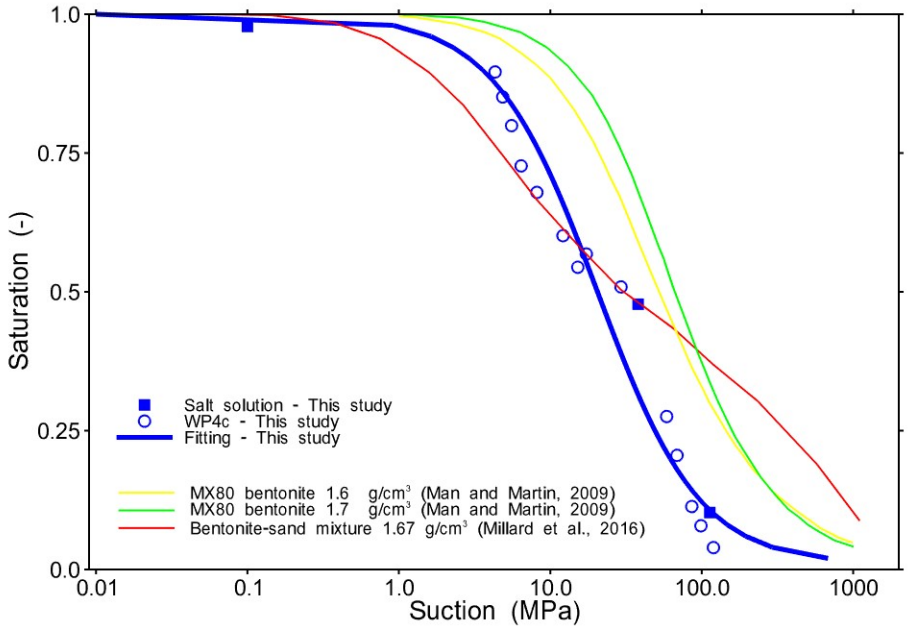

Figure 4. WRC of bentonite–sand mixture of this study with a fitted van Genuchten curve, compared with other studies [44,45].

Table 3. The basic properties of used materials.

Property	Description
Bentonite	
Specific gravity (G_s)	2.71
Liquid limit (%)	493%
Plastic limit (%)	41%
Plasticity index	452%
Content of the <2 μm fraction (%)	67%
Cation exchange capacity (meq/100 g)	75%
Free swelling index (%)	1578.5%
Main mineral components	Montmorillonite (75%) Illite (5%) Feldspar and Quartz (<3%)
Sand	
Specific gravity (Gs)	2.66
Cu	2
Cc	1.4
Main chemical components	SiO_2 (95%)
Parameters of WRC fitted model (70-30 bentonite-sand)	
m	0.47
n	1.89
α	6.5×10^{-8}
S_l	0.01

The fitted WRC of this study also was compared to the fitted WRC obtained in other investigations on the compacted bentonite and bentonite–sand mixture of similar density, as shown in Figure 4 [44,45]. The comparison shows that the obtained fitted WRC of this study is in good agreement with other WRC results in term of general shape (range of fitting parameters); however, the WRC of this study showed lower residual liquid saturation.

2.2. Specimen Preparation

In this study, experiments were performed on samples of a compacted mixture of 70-30 bentonite-sand, with a dry density of 1.65 g/cm^3. To prepare the specimens, the materials were dried in the oven at the standard temperature of 105 °C for 24 h, based on the ASTM D2216-19 [46]; after that, the required weight of oven-dried sand was added to oven-dried bentonite. Subsequently, the dry materials were initially mixed by hand and then de-aired distilled water was sprayed in several stages to achieve 7% of the water content. The materials were mixed by hand until reaching a uniform mixture, and then, the prepared mixtures were stored in sealed plastic bags for 24 h to reach equilibrium. The prepared mixtures were statically compacted to the desired density and degree of water saturation (30%) in a designed split cylindrical steel mold at a controlled load rate, using an INSTRON Universal Testing System to reach the target cylindrical specimen of the HM column test, with a diameter of 49 mm and a height of 100 mm, as shown in Figure 5.

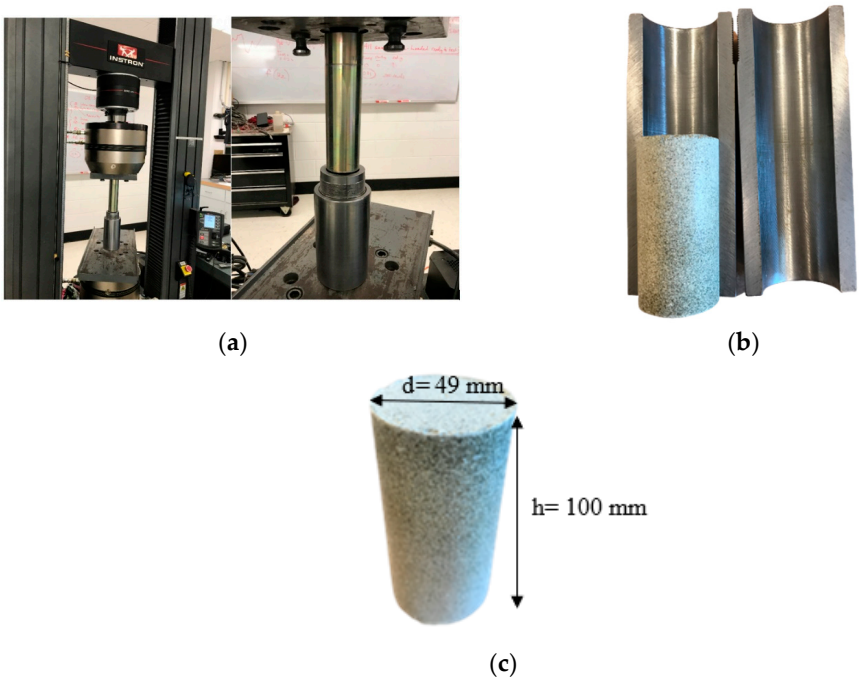

Figure 5. (**a**) Sample preparation using the INSTRON Universal Testing System; (**b**) compacted sample in the split cylinder mold; (**c**) the sample dimensions.

2.3. Design of HM Column Type Test

The design layout of the HM column type test is shown in Figure 6a. The test setup's configuration included a bronze cylindrical cell, modified GDS dynamic triaxial testing equipment, four small pressure sensors (PS) at various heights, and three sealed holes with bolts to allow for more sensors to be added in the future. In this study, 7.6 mm in diameter and 2 mm in thickness PDB-PB miniature pressure transducers, provided by Tokyo Measuring Instruments Lab, were used. These sensors are ultracompact, lightweight, optimal for model testing, and waterproof, with a capacity of 3 MPa [47]. The cylindrical cell has a diameter of 50 mm and a height of 155 mm. Any radial deformation would be blocked by the rigid structure of the cylindrical cell. The top cap, with a diameter of 49 mm, is placed on the top of the sample within the 50 mm diameter cylindrical cell with

a gap of 1 mm to reduce the friction between the top cap and cell during the test and to provide a space for gas to escape during the hydration. The top cap is made of lightweight Perspex, with a modulus of elasticity two orders of magnitude higher than the compacted bentonite–sand mixture, making elastic deformation of the top cap negligible.

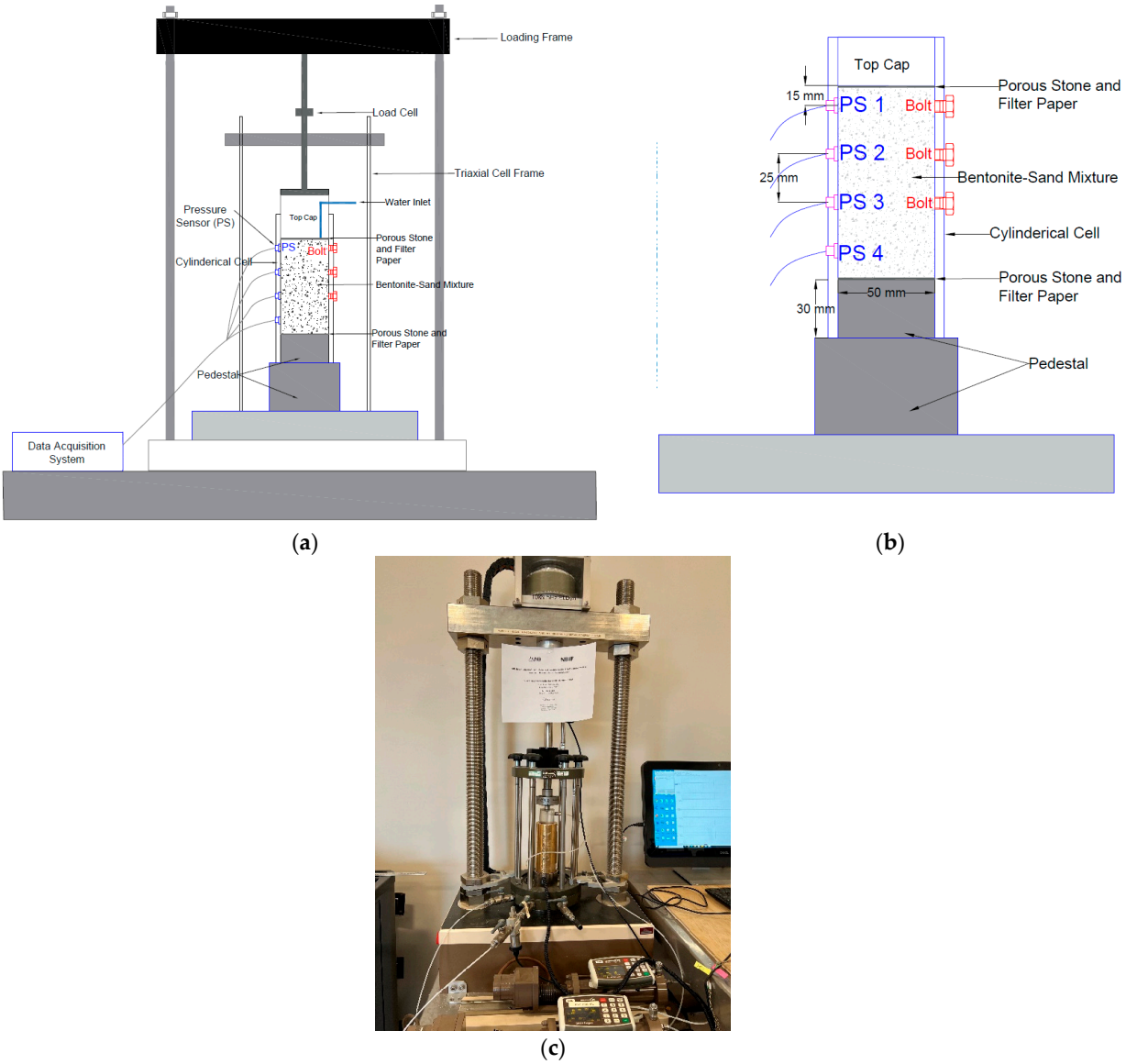

Figure 6. (**a**) Design layout of HM column test; (**b**) schematic of cylindrical cell and sensors; (**c**) the cylindrical cell equipped by sensors in triaxial setup.

The 10 kN self-control triaxial GDS apparatus system is based on an axially stiff-loaded frame with an electromechanical actuator (GDS Instruments Ltd., Hook, UK) capable of performing the constant-volume (CV) experiments by preventing the vertical swelling, using a rigid reaction frame with a force transducer. In this study, the triaxial cell was modified to connect the sensors to the data acquisition system through the triaxial cell.

The pressure sensors are located at different heights of the sample (h = 15, 40, 65, and 90 mm) to measure the radial swelling pressure, as shown in Figure 6b,c.

2.4. The Procedure of the HM Column-Type Test

The compacted BBSM was carefully placed into the cylindrical cell with porous stones and filter papers on the top and bottom, as shown in Figure 7. The cylindrical cell was then inserted into the GDS triaxial frame. The top cap was connected with a water inlet to

allow the samples to be hydrated from the top of the sample, with a pressure of 5 kPa, at constant vertical position conditions. It should be mentioned that the experiments were performed in the parallel direction to compaction direction. Following the completion of the hydration test, the sample was gently pushed out by steel bars attached to a frame, as shown in Figure 8. The extracted samples were sliced using a cutter and band saw into different sections, and the wet weight and volume of each section were measured. The water content and saturation of each section were measured after oven drying for 24 h at 105 °C, and the wetting front for each sample were determined. In this study, five identical samples were tested with different testing time duration (1 day, 2 days, 8 days, 30 days, and 120 days). The extracted sample after 120 days of testing is shown in Figure 9a, and a section of the sample is shown in Figure 9b. The procedure described here is consistent with the procedure of Villar [48] and Yong et al. [29].

Figure 7. The compacted sample inside the cylindrical cell.

Figure 8. Extraction of the sample after termination of each test.

(**a**) (**b**)

Figure 9. (**a**). Extracted sample after 120 days; (**b**) a section of cut sample.

3. Results and Discussion

3.1. Evolution of the Wetting Profile

Figure 10a illustrates a compacted sample prior to the test, and Figure 10b–f shows the extracted samples at the end of each HM column-type test in different durations of experiments. In Figure 10, the wetting front advancing after each test has been marked, indicating the visual observation of the advancement of the wetting profile, which progressed more than half of the height of the sample in 120 days.

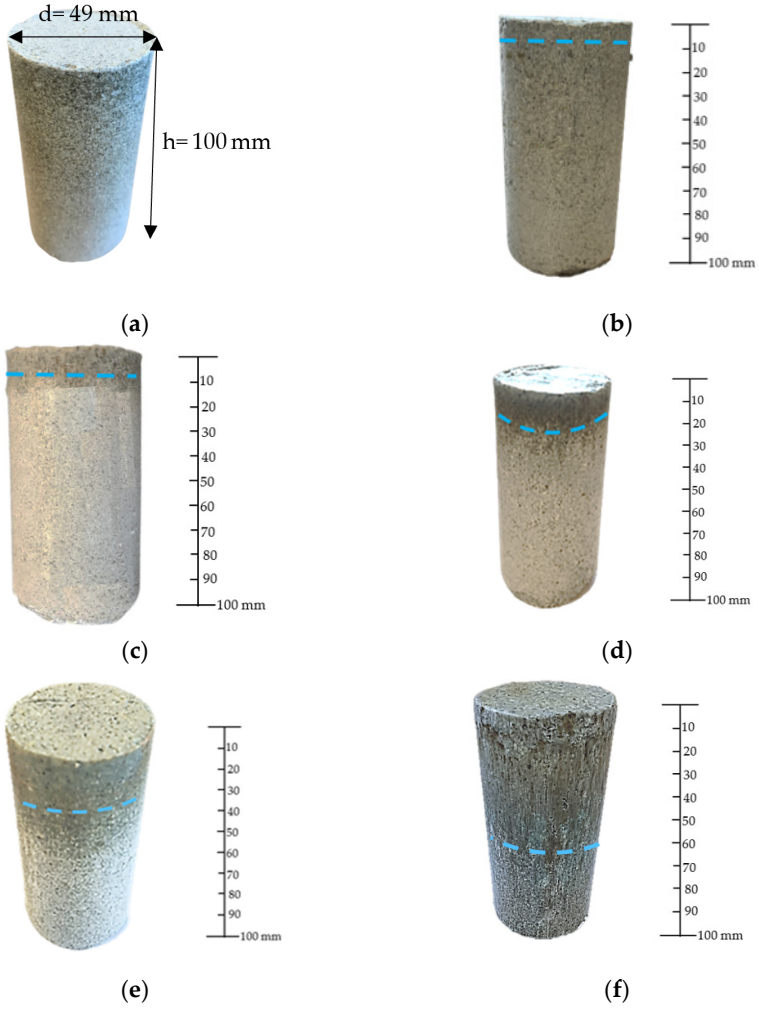

Figure 10. Evolution of wetting profile of bentonite–sand (70-30) for different testing time durations (**a**) initial; (**b**) after 1 day of hydration; (**c**) after 2 days of hydration; (**d**) after 8 days of hydration; (**e**) after 30 days of hydration; (**f**) after 120 days of hydration.

The water saturation along the height of each sample at the end of each HM column-type test was derived from the wet weight and volume of each slice, and then, the advancement of the wetting profile of each test was obtained to confirm the visual observation of the evolution of the wetting profile. Figure 11 shows the variation of the water saturation along the sample height for all five tests. After 120 days of infiltration, an overall increase in the degree of saturation is observed in the sample, and the advancement of the wetting profile has progressed to almost 57 mm from the hydration front. It should be noted that each time duration (1, 2, 8, 30, and 120 days) was tested using one representative sample, therefore no error bars are shown on Figure 11. The measured advancement of the wetting profile of each test is presented in Table 4.

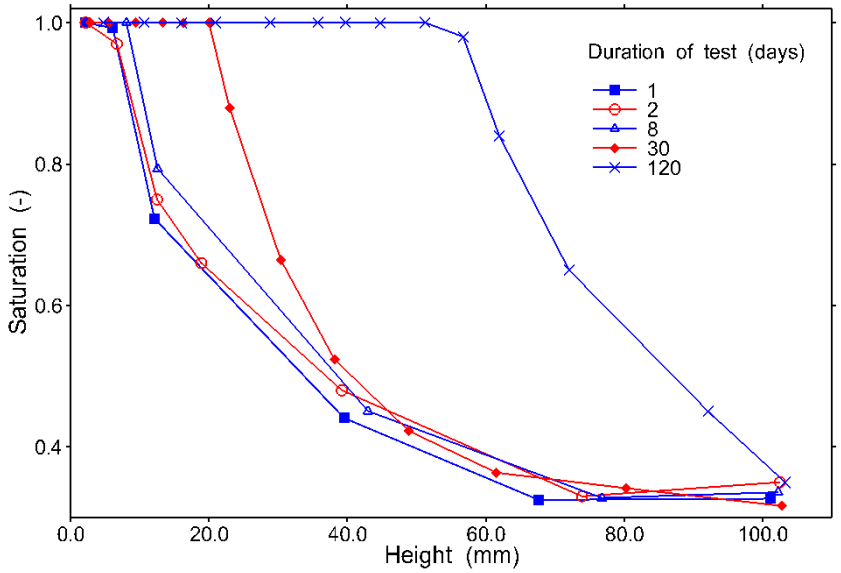

Figure 11. Wetting profile along the sample at different time durations, as derived from the wet weight and volume of slices.

Table 4. Advancement of wetting front.

Time (Day)	Distance from Hydration Front (mm)
1	6.13
2	6.7
8	8.08
30	20
120	56.75

Figure 12 shows the amount of water intake versus the time of different HM column-type experiments, measured by the water inlet device, while performing the experiments with a zoom on the first 10 days. The increase in the amount of water intake was rapid at the earlier stage of all of the experiments and then gradually decreased. The rapid rate could be attributed to the initial conditions of porous stones, which were dry (volume increase in water intake of all of the experiments was almost 5000 mm^3, and the volume of voids for porous stone was 4400 mm^3). Figure 12 further illustrates that the rate of infiltrated water for all of the experiments are comparable, which indicates the samples were identical.

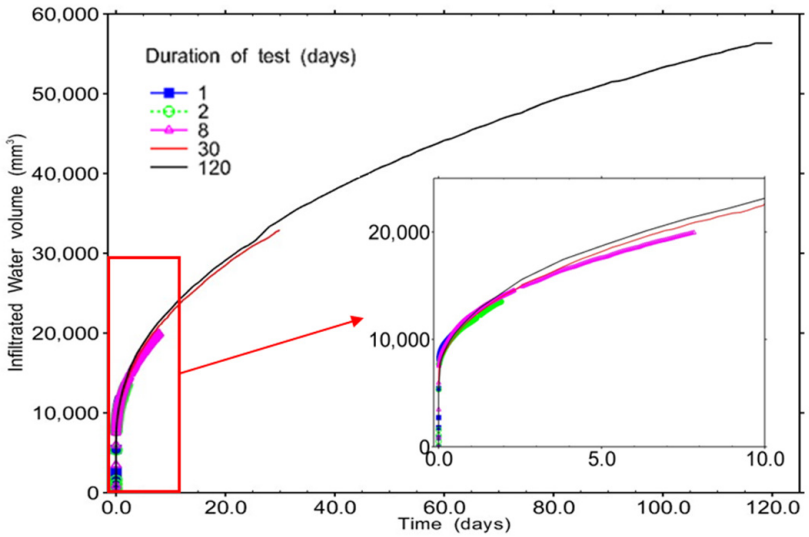

Figure 12. Infiltrated water volume into the BBSM samples with a zoom on the first 10 days.

Figure 13 compares the volume of water recorded by the water inlet device with the volume of water derived from saturation measurements. Both independent values fairly coincide.

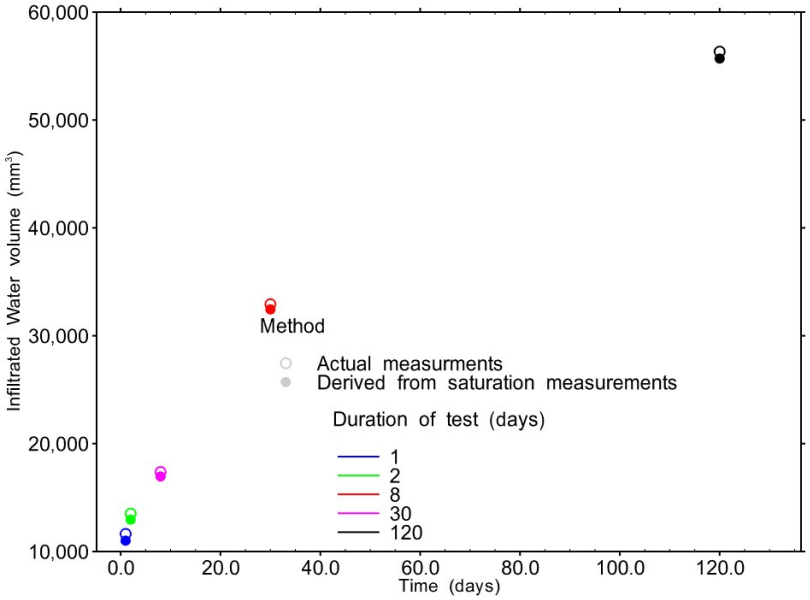

Figure 13. Actual measured infiltrated water volume compared to water volume derived from saturation measurements in different sections after each test.

3.2. Evolution of Axial and Radial Swelling Pressure

The results of axial swelling pressures versus time are presented in Figure 14. The evolution of swelling pressure during the hydration process shows the same pattern for all of the experiments, in which, at the early stage, the axial swelling pressure increases rapidly, followed by a period with a continuous but slow increase in swelling pressure. In this study, even after 120 days of testing, peak value and stabilization of axial pressure was not observed.

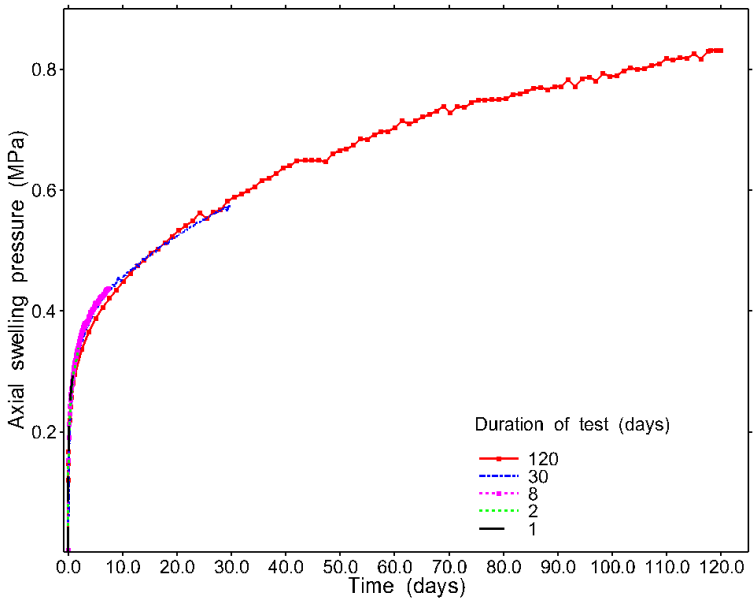

Figure 14. Evolution of axial swelling pressure during different times.

The reason for the previously mentioned behavior of the evolution pattern of axial swelling pressure can be explained by the structure of compacted BBSM, which has been studied from various perspectives. For example, several studies investigated the sealing mechanism and induced swelling of clay rock formation, namely, Opalinus Clay, around a fractured zone, such as the Excavation Damaged Zone (EDZ), surrounding the underground structure of the DGR using different techniques of mapping and scanning [49–51]. Laurich et al. [49] studied the closure of an artificial fracture in a sample of Opalinus Clay during the injection of water by means of 2D strain mapping. The observation of this study indicated that the sealing and swelling process involved two main aspects: localized volume increase and distributed volume increase. The localized volume, which can occur when tiny pre-existing cracks expand, caused the rock slabs to move and the crack to close. This process happened quickly and reduced the initial crack size. The distributed volume increase process was slower and involved a gradual expansion of the wetting front by diffuse wetting [49].

By starting the hydration, a high hydraulic gradient between the top boundary and the high initial negative pore water pressure of the sample will force the water to infiltrate the top layer of the sample. Within this top layer, water initially goes into the inter-aggregate pores and the preliminary swelling state starts until the macro-pores are filled with swelling intra-elements, resulting in the swelling of bentonite grains and leading to the advanced state and a sudden and significant rise in the swelling pressure. In this state, clay particles keep attracting the water to form a diffuse double layer (diffuse wetting) [11,49]. The diffuse wetting will push the particles apart, resulting in a new pore size distribution with an increase in micro-porosity and a reduction in macro-porosity. The transition of pore size distribution from macro-porosity dominating to micro-porosity dominating causes a decrease in the rate of swelling pressure [11]. Porosity changes can be interpreted as changes in total permeability. Therefore, by continuing the wetting process and increasing the degree of saturation, the permeability of BBSM will be reduced, which will result in a lower rate of swelling pressure. This could also explain the slow rate of infiltrated water as shown in Figure 12.

As seen in Figure 14, the axial swelling pressure difference for all HM-column type tests was negligible, demonstrating the similarity and comparability of the samples. After 30 days, the measured axial swelling pressure was 0.57 MPa and increased after 120 days by 46% to 0.83 MPa. Among the five time durations of the experiments, the 30-day and 120-day tests were selected for discussion of axial swelling pressure because the 30-day test

showed a greater advancement of the wetting profile than the 1, 2, and 8-day experiments, and 120 days showed the maximum swelling pressure.

Figure 15 shows the schematic of the cylindrical cell with locations of all of the sensors and the advancement of the wetting front of all HM column-type tests, along with the swelling pressure evolution for radial pressure sensors (PS1, PS2, PS3, PS4) and axial pressure sensors for 120 days.

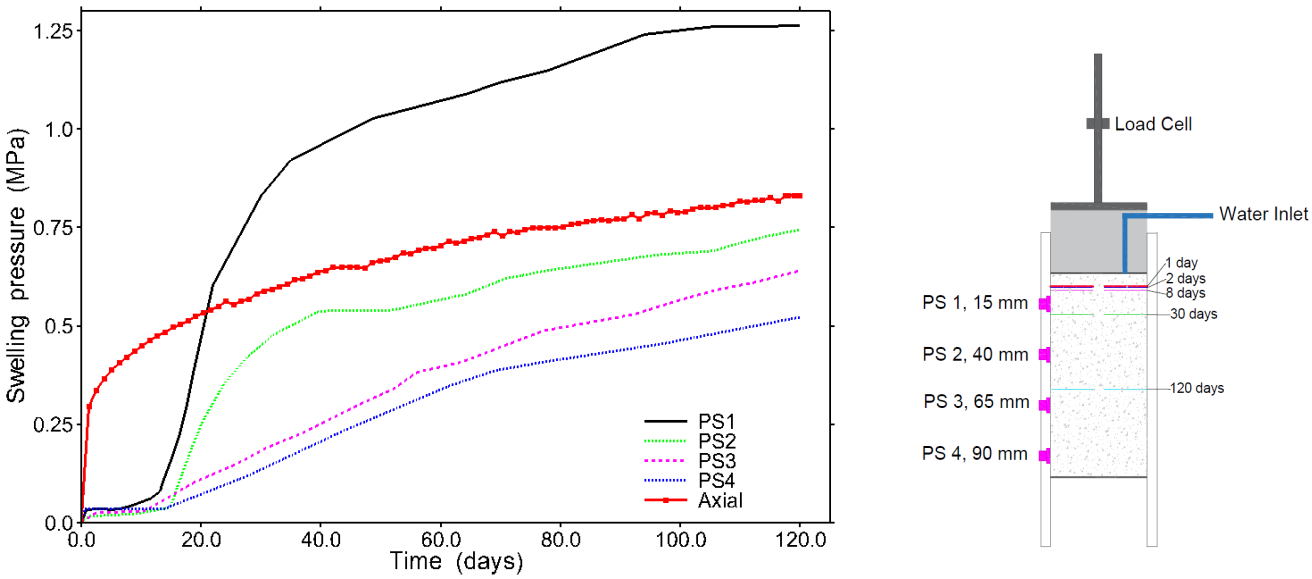

Figure 15. Location of sensors and advancement of wetting front, and radial and axial swelling pressure for 120 days.

Although a quick increase was observed for axial swelling pressure, the radial swelling pressures showed a lower initial increase rate. The small amount of radial swelling pressure during the first several days of hydration may be explained by comparing the locations of the sensors with the progression of the wetting front, as depicted in Figure 15. PS1 was placed 15 mm from the hydration front along the height of the sample, and the progression of the wetting front of the initial 1, 2, and 8 days occurred before the location of the PS1 at 15 mm.

After the early stages, all of the radial pressure sensors showed an increase in the swelling pressure. The rate of increase for each radial pressure sensor is different. A higher rate of radial swelling pressure was found for the sensors located closer to the top of the sample and hydration front, which is PS1. The portions near the hydration front absorb water quickly, causing swelling pressure to rise at a faster rate; at the same time, the reduction in permeability reduced the amount of water flowing downward, hence, reducing the rate of swelling. This behavior was observed in the evolution of axial swelling pressure and infiltrated water volume, as shown in Figures 12 and 14.

In the 30-day HM column-type test, the PS1 sensor measured 0.59 MPa. In the 120-day test, PS1 reached a peak value and stabilization at about 1.26 MPa, which is 52% higher than the measurement of the axial swelling pressure after 120 days. The swelling pressure anisotropy in BBSM has been observed in some previous experimental studies [52–55], as well as in situ experiments such as in situ tests of the SEALEX experiments [21]. In this study, one possible explanation for the difference in peak values between radial and axial swelling pressure can be attributed to the presence of side friction between the sample and cell along the axial direction. Saba et al. [55] performed a series of experiments on the compacted mixture of bentonite–sand and analyzed the samples using microfocus X-ray computed tomography (μCT). Image analysis of the work of Saba et al. [55] revealed a concentration of macro-pores at the radial border due to the sample preparation, which could explain why the radial swelling pressure peak was larger than the axial one. In this

study, the radial heterogeneity could also explain the larger radial swelling pressure, which should be investigated further in future experiments.

PS2 showed the second highest rate of radial swelling pressure in the 30- and 120-day experiments, with an evolution similar to PS1 but with a lower and smoother final value. The swelling pressure measured at the sensors PS3 and PS4 increased at similar rates at the beginning, with a slightly higher value for PS3.

As mentioned before, the swelling pressure of BBSM could exert on the host rock formation and have influence on the stability of the DGR system. The estimation of in situ stress components of the host rock is an essential factor of DGR's design, which depends on the type of geological formation selected in different radioactive waste management organizations. For example, the in situ principal minor stress is 3–4 MPa at the Tournemire site in France [56], 4–5 MPa at the Mol site in Belgium [57], and 7 MPa at the Bure site in France [58]. The axial and radial swelling pressures of BBSM observed during the 120-day test in this study were found to be lower than the range of in situ stress of various rock formations; however, it is important to consider the results of long-term swelling pressure in conditions of complete saturation and long-term durations when designing a DGR system.

Figure 16 shows the evolution of the swelling pressure profile at different days (1, 2, 8, 30, and 120 days) of the experiment with the location of wetting front advancement. The swelling pressure at the top of the sample (PS1) showed a higher value. However, the swelling pressure along the other locations showed a uniform increase and was expected to continue increasing until an equilibrium occurs.

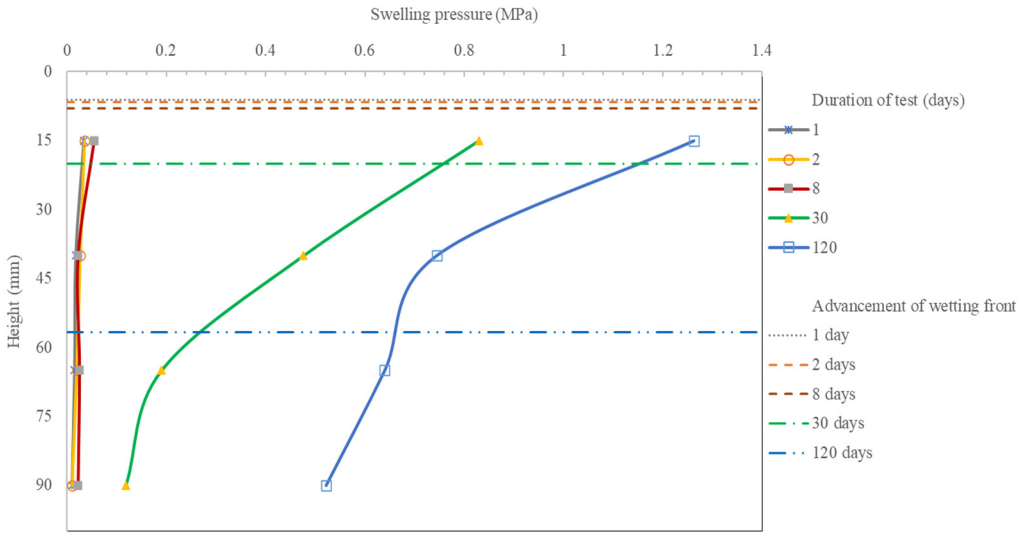

Figure 16. Evolution of radial swelling pressure along the height of sample in 120-day test.

4. Conclusions

Five HM column-type tests were performed on a mixture of 70-30 bentonite-sand at a dry density of 1.65 g/cm^3 to investigate the early stages of the swelling behavior of BBSM as a sealing material of an engineered barrier system of DGR. The experiments were conducted in parallel with compaction direction at room temperature by supplying distilled water from the top of the sample for different durations (between 1 day and 120 days). The evolution of axial and radial swelling pressures, along with the volume of water intake, were measured by various sensors.

In addition to the development of swelling pressures at different directions, the water saturation and the advancement of the wetting front were observed and measured along the sample by slicing each sample into different sections at the end of each HM column-type experiment. After 120 days of the HM column-type test, two zones can be observed. The first zone was the fully saturated zone, from the top of the sample to the wetting front, at 57 mm. At this zone, the water saturation increased from 30% to 100%. The second

zone was still undersaturated, with water saturation ranging from 30% (at the bottom of the sample) to 100% (at the wetting front) gradually. The volume of water intake was derived from the difference between each section's final and initial water content, which was confirmed by the water intake measured by the automatic volume change apparatus. All of the samples used for the five test durations were prepared to be identical samples. The volume of water intake for all of the tested samples showed identical rates when plotted in the same graph, confirming the samples' similarity.

During the hydration of BBSM samples, the axial swelling pressure showed a quick increase, followed by a slower increase. This observation could be explained by the changes in structure of BBSM in different swelling states. In the preliminary swelling state, water entered the inter-aggregate pores from the top layer of the sample until it filled up the macro-pores with swelling intra-elements. This led to the advanced swelling state, with a sudden and significant increase in the swelling pressure. In the advanced swelling state, the diffuse wetting forced the particles apart, resulting in an increase in micro-porosity and a decrease in macro-porosity, which reduced the rate of swelling pressure.

The findings also indicate that the development of radial swelling pressure differs from axial swelling pressure. The evolution of axial swelling pressure showed an initial increase in swelling pressure for all of the experiments, while the radial swelling pressure showed a lower initial increase. After the early stages, all of the radial sensors showed an increase in swelling pressure. In the 120-day experiment, the axial swelling pressure increased to 0.83 MPa, and the radial pressure sensor close to the hydration front measured 1.26 MPa, 52% higher than the axial swelling pressure. One possible explanation for the swelling pressure anisotropy could be associated with the side friction between the cell and sample, causing the decrease in axial swelling pressure. The potential friction between the sample and the cylindrical cell can be considered in future studies. Another explanation for this observation could be due to the heterogeneity of the sample resulting in a looser border in radial direction of the sample which could be further investigated in future studies using a scanning method. In addition to identifying the density and pore size distribution in axial and radial directions through scanning analysis, scanning of the samples could also assist in identify the change in orientation of bentonite grains, which could explain the anisotropy in swelling pressure.

The obtained results of swelling pressures of BBSM in this study during the 120-day test were lower than the range of reported in situ stress of different rock formations, and moreover, these values were also close to the minimum criteria required to prevent microbial activity and minimize advection, indicating no significant safety issue in the system. However, when designing a DGR system, it is essential to consider the swelling pressures in full complete saturation and long-term durations. Additionally, it is crucial to recognize the distinctions between field and experimental conditions, including the different water supply rates in the laboratory and in situ environments.

The present study has provided comprehensive investigations of bentonite materials' swelling behaviors during the hydration process. Future studies of exploring the effects of chemical solutions of injected water and elevated temperature on the swelling pressure of bentonite could be conducted to simulate more practical field conditions.

Author Contributions: Methodology, O.N.; investigation, M.S.B.; writing—original draft, M.S.B.; writing—review and editing, O.N.; supervision, O.N.; funding acquisition, W.T.O. All authors have read and agreed to the published version of the manuscript.

Funding: The experimental equipment of this study was funded partially by the New Brunswick Innovation Foundation (NBIF EQP2021-005). The authors are grateful to the NBIF for the financial support.

Data Availability Statement: Data are contained within the article.

Conflicts of Interest: The authors declare no conflict of interest.

References

1. Wang, Q.; Tang, A.M.; Cui, Y.J.; Delage, P.; Gatmiri, B. Experimental study on the swelling behaviour of bentonite/claystone mixture. *Eng. Geol.* **2012**, *124*, 59–66. [CrossRef]
2. NWMO. Available online: https://www.nwmo.ca/ (accessed on 1 August 2022).
3. ANDRA. Available online: https://www.andra.fr/ (accessed on 30 May 2022).
4. SKB. Available online: https://www.skb.com/ (accessed on 30 May 2022).
5. Ojovan, M.I.; Lee, W.E. *An Introduction to Nuclear Waste Immobilisation*; Elsevier: Amsterdam, The Netherlands, 2014; ISBN 9780080444628.
6. NWMO. *RD 2019—NWMO' s Program for Research and Development for Long-Term Management of Used Nuclear Fuel*; NWMO: Toronto, ON, Canada, 2019; ISBN 4169349814.
7. Sun, D.; Cui, H.; Sun, W. Swelling of compacted sand-bentonite mixtures. *Appl. Clay Sci.* **2009**, *43*, 485–492. [CrossRef]
8. *ASTM D4546-14*; Standard Test Methods for One-Dimensional Swell or Collapse of Cohesive Soils. Astm: West Conshohocken, PA, USA, 2014; pp. 1–9.
9. Mitchell, J.K.; Soga, K. *Fundamentals of Soil Behavior*; John Wiley & Sons: New York, NY, USA, 2005; Volume 3, ISBN 978-0-471-46302-3.
10. Rawat, A. Coupled Hydro-mechanical Behavior of a Compacted Bentonite-Sand Mixture: Experimental and Numerical Investigations. Doctoral Dissertation, Faculty of Civil and Environmental Engineering Ruhr-Universität Bochum, Bochum, Germany, 2019.
11. Nasir, O.; Calder, N.; Walsh, R.; Avis, J.; Engineering, G.; Kremer, E.P. A Concept for Modelling Evolution of Permeability in Re-hydrating Bentonite. In Proceedings of the 70th Canadian Geotechnical Conference (GeoOttawa 2017), Ottawa, ON, Canada, 1–4 October 2017.
12. Seiphoori, A.; Ferrari, A.; Laloui, L. Water retention behaviour and microstructural evolution of MX-80 bentonite during wetting and drying cycles. *Geotechnique* **2014**, *64*, 721–734. [CrossRef]
13. Nasir, O.; Nguyen, T.S.; Barnichon, J.D.; Millard, A. Simulation of hydromechanical behaviour of bentonite seals for containment of radioactive wastes. *Can. Geotech. J.* **2017**, *54*, 1055–1070. [CrossRef]
14. Briggs, S.; Krol, M. *Diffusive Transport Modelling of Corrosion Agents through the Engineered Barrier System in a Deep Geological Repository for Used Nuclear Fuel-NWMO-TR-2018-06*; NWMO: Toronto, ON, Canada, 2018.
15. Martino, J.B.; Dixon, D.A.; Kozak, E.T.; Gascoyne, M.; Vignal, B.; Sugita, Y.; Fujita, T.; Masumoto, K. The tunnel sealing experiment: An international study of full-scale seals. *Phys. Chem. Earth* **2007**, *32*, 93–107. [CrossRef]
16. Lanyon, G.W.; Gaus, I. *Main Outcomes and Review of the FEBEX In Situ Test (GTS) and Mock-Up after 15 Years of Operation*; National Cooperative for the Disposal of Radioactive Waste (NAGRA): Wettingen, Switzerland, 2016; ISSN 1015-2636.
17. Van Geet, M.; Bastiaens, W.; Volckaert, G.; Weetjens, E.; Sillen, X.; Gens, A.; Villar, M.V.; Imbert, C.; Filippi, M.; Plas, F. Installation and evaluation of a large-scale in-situ shaft seal experiment in Boom clay—The RESEAL project. In Proceedings of the International Conference on Clays in Natural and Engineered Barriers for Radioactive Waste Confinement, Lille, France, 17–18 September 2007.
18. Van Geet, M.; Bastiaens, W.; Volckaert, G.; Vallejan, B.; Gens, A.; Villar, M.V.; Mingarro, M.; Caron-Charles, M.; Imbert, C.; Plas, F. Large scale in situ demonstration test for repository sealing in an argillaceous host rock-The RESEAL project. 2004. In Proceedings of the International Conference on the Management and Disposal of Radioactive Waste. Radioactive Waste Management—Community Policy and Research Initiatives, Luxembourg, Luxembourg, 29–31 March 2004.
19. Mayor, J.C.; García-Siñeriz, J.L.; Rey, M. *Engineered Barrier Emplacement Experiment in Opalinus Clay for the Disposal of Radioactive Waste in Underground Repositories*; Empresa Nacional de Residuos, S.A., ENRESA: Madrid, Spain, 2005.
20. Thatcher, K.E.; Bond, A.E.; Robinson, P.; McDermott, C.; Fraser Harris, A.P.; Norris, S. A new hydro-mechanical model for bentonite resaturation applied to the SEALEX experiments. *Environ. Earth Sci.* **2016**, *75*, 1–17. [CrossRef]
21. Wang, Q.; Tang, A.M.; Cui, Y.J.; Barnichon, J.D.; Ye, W.M. A comparative study on the hydro-mechanical behavior of compacted bentonite/sand plug based on laboratory and field infiltration tests. *Eng. Geol.* **2013**, *162*, 79–87. [CrossRef]
22. Millard, A.; Mokni, N.; Barnichon, J.D.; Thatcher, K.; Bond, A.; Fraser-Harris, A.; Mc Dermott, C.; Blaheta, R.; Michalec, Z.; Hasal, M.; et al. Comparative modelling approaches of hydro-mechanical processes in sealing experiments at the Tournemire URL. *Environ. Earth Sci.* **2017**, *76*, 78. [CrossRef]
23. Fraser Harris, A.P.; McDermott, C.I.; Bond, A.E.; Thatcher, K.; Norris, S. A nonlinear elastic approach to modelling the hydro-mechanical behaviour of the SEALEX experiments on compacted MX-80 bentonite. *Environ. Earth Sci.* **2016**, *75*, 1445. [CrossRef]
24. Millard, A.; Barnichon, J.D.; Mokni, N.; Thatcher, K.E.; Bond, A.; Blaheta, R. Modelling benchmark of a laboratory test on hydro-mechanical behavior of bentonite. In Proceedings of the UNSAT 2014: International Conference on Unsaturated Soils: Research and Applications, Sydney, Australia, 2–4 July 2014; Volume 1, pp. 489–495. [CrossRef]
25. Schanz, T.; Nguyen-Tuan, L.; Datcheva, M. A column experiment to study the thermo-hydro-mechanical behaviour of expansive soils. *Rock Mech. Rock Eng.* **2013**, *46*, 1287–1301. [CrossRef]
26. Rawat, A.; Baille, W.; Tripathy, S. Swelling behavior of compacted bentonite-sand mixture during water infiltration. *Eng. Geol.* **2019**, *257*, 105141. [CrossRef]
27. Åkesson, M.; Jacinto, A.C.; Gatabin, C.; Sanchez, M.; Ledesma, A. Bentonite THM behaviour at high temperatures: Experimental and numerical analysis. *Geotechnique* **2009**, *59*, 307–318. [CrossRef]

28. Pintado, X.; Ledesma, A.; Lloret, A. Backanalysis of thermohydraulic bentonite properties from laboratory tests. *Eng. Geol.* **2002**, *64*, 91–115. [CrossRef]
29. Yong, R.N.; Mohamed, A.M.O.; Shooshpasha, I.; Onofrei, C. Hydro-thermal performance of unsaturated bentonite-sand buffer material. *Eng. Geol.* **1997**, *47*, 351–365. [CrossRef]
30. Graupner, B.J.; Shao, H.; Wang, X.R.; Nguyen, T.S.; Li, Z.; Rutqvist, J.; Chen, F.; Birkholzer, J.; Wang, W.; Kolditz, O.; et al. Comparative modelling of the coupled thermal–hydraulic-mechanical (THM) processes in a heated bentonite pellet column with hydration. *Environ. Earth Sci.* **2018**, *77*, 1–16. [CrossRef]
31. Villar, M.V.; Martín, P.L.; Romero, F.J. Long-term THM tests reports: THM cells for the HE-E test: Update of results until February 2014 CIEMAT Technical Report CIEMAT. *PEBSDeliverable D2.2-7.3.* **2014**, *2014*, 22.
32. Gatabin, C.; Robinetz, J.C.; Plas, F.; Vignal, B.; Lassabatere, T. Bentonite THM behaviour mock-up studies. In Proceedings of the Clays in Natural and Engineered Barriers for Radioactive Waste Confinement, Tours, France, 14–18 March 2005; p. 723.
33. Cuevas, J.; Villar, M.V.; Fernández, A.M.; Gómez, P.; Martín, P.L. Pore waters extracted from compacted bentonite subjected to simultaneous heating and hydration. *Appl. Geochem.* **1997**, *12*, 473–481. [CrossRef]
34. Cui, Y.J.; Tang, A.M.; Loiseau, C.; Delage, P. Determining the unsaturated hydraulic conductivity of a compacted sand-bentonite mixture under constant-volume and free-swell conditions. *Phys. Chem. Earth* **2008**, *33*, 462–471. [CrossRef]
35. Saba, S.; Cui, Y.; Tang, A.M.; Barnichon, J. Investigation of the swelling behaviour of compacted bentonite–sand mixture by mock-up tests. *Can. Geotech. J.* **2014**, *51*, 1399–1412. [CrossRef]
36. Wang, Q.; Cui, Y.J.; Tang, A.M.; Barnichon, J.D.; Saba, S.; Ye, W.M. Hydraulic conductivity and microstructure changes of compacted bentonite/sand mixture during hydration. *Eng. Geol.* **2013**, *164*, 67–76. [CrossRef]
37. Liu, Z.R.; Cui, Y.J.; Ye, W.M.; Chen, B.; Wang, Q.; Chen, Y.G. Investigation of the hydro-mechanical behaviour of GMZ bentonite pellet mixtures. *Acta Geotech.* **2020**, *15*, 2865–2875. [CrossRef]
38. Bentonite Performance Minerals LLC (BPM). Available online: https://www.bentonite.com/bpm/default.html (accessed on 10 July 2020).
39. *ASTM C837-09*; Standard Test Method for Methylene Blue Index of Clay. Astm: West Conshohocken, PA, USA, 2009.
40. Sivapullaiah, P.V.; Sitharam, T.G.; Subba Rao, K.S. Modified Free Swell Index for Clays. *Geotech. Test. J.* **1987**, *10*, 80–85.
41. Shaw Resources. Available online: https://shawresources.ca/blog/2019/04/23/silica-sand-different-regular-sand/ (accessed on 10 July 2020).
42. METER Group Inc. USA WP4C. Available online: https://www.metergroup.com/ (accessed on 1 May 2021).
43. van Genuchten, M.T. Closed-Form Equation for Predicting the Hydraulic Conductivity of Unsaturated Soils. *Soil Sci. Soc. Am. J.* **1980**, *44*, 892–898. [CrossRef]
44. Millard, A.; Mokni, N.; Barnichon, J.D.; Thatcher, K.E.; Bond, A.E.; Fraser-Harris, A.; Mc Dermott, C.; Blaheta, R.; Michalec, Z.; Hasal, M.; et al. Comparative modelling of laboratory experiments for the hydro-mechanical behaviour of a compacted bentonite–sand mixture. *Environ. Earth Sci.* **2016**, *75*, 1311. [CrossRef]
45. Man, A.; Martino, J.B. *Thermal, Hydraulic and Mechanical Properties of Sealing Materials*; NWMO TR-2009-20; NWMO: Toronto, ON, Canada, 2009; ISBN 4169349814.
46. *ASTM D2216-19*; Standard Test Methods for Laboratory Determination of Water (Moisture) Content of Soil and Rock by Mass. Astm: West Conshohocken, PA, USA, 2019.
47. Tokyo Measuring Instruments Lab. Available online: https://tml.jp/e/product/transducers/pda_pdb.html (accessed on 1 November 2023).
48. Villar, M.V. Infiltration tests on a granite/bentonite mixture: Influence of water salinity. *Appl. Clay Sci.* **2006**, *31*, 96–109. [CrossRef]
49. Laurich, B.; Fourrière, A.; Graesle, W. TN 2020-29 LT-A Experiment: How Fracture Wetting Leads to Closure; 2019. Available online: https://www.researchgate.net/publication/339528075_TN_2020-29_LT-A_Experiment_How_fracture_wetting_leads_to_closure/ (accessed on 30 September 2023).
50. Voltolini, M.; Ajo-Franklin, J.B. The Sealing Mechanisms of a Fracture in Opalinus Clay as Revealed by in situ Synchrotron X-ray Micro-Tomography. *Front. Earth Sci.* **2020**, *8*, 207. [CrossRef]
51. Seiphoori, A. Arbeitsbericht NAB 19-07 Self-sealing of fractures in Opalinus Clay: Experiments and a conceptual framework for quantitative assessments. *National Cooperative for the Disposal of Radioactive Waste (NAGRA), Wettingen, Switzerland.* **2019**, *103*.
52. Lee, J.O.; Lim, J.G.; Kang, I.M.; Kwon, S. Swelling pressures of compacted Ca-bentonite. *Eng. Geol.* **2012**, *129–130*, 20–26. [CrossRef]
53. Cho, W.J.; Lee, J.O.; Kang, C.H. Influence of temperature elevation on the sealing performance of a potential buffer material for a high-level radioactive waste repository. *Ann. Nucl. Energy* **2000**, *27*, 1271–1284. [CrossRef]
54. Lee, J.; Cho, W.; Chun, K. Swelling pressures of a potential buffer material for high-level waste repository. *J. Korean Nucl. Soc.* **1999**, *31*, 139–150.
55. Saba, S.; Barnichon, J.D.; Cui, Y.J.; Tang, A.M.; Delage, P. Microstructure and anisotropic swelling behaviour of compacted bentonite/sand mixture. *J. Rock Mech. Geotech. Eng.* **2014**, *6*, 126–132. [CrossRef]
56. Barnichon, J.-D.; Deleruyelle, F. Sealing experiments at the Tournemire URL. In *Towards Convergence of Technical Nuclear Safety Practices in Europe*; Eurosafe Forum: Bruxelles, Belgium, 2009.

57. Li, X.L.; Bastiaens, W.; Van Marcke, P.; Verstricht, J.; Chen, G.J.; Weetjens, E.; Sillen, X. Design and development of large-scale in-situ PRACLAY heater test and horizontal high-level radioactive waste disposal gallery seal test in Belgian HADES. *J. Rock Mech. Geotech. Eng.* **2010**, *2*, 103–110. [CrossRef]
58. Delage, P.; Cui, Y.-J.; Tang, A.M. Clays in radioactive waste disposal. *J. Rock Mech. Geotech. Eng.* **2010**, *2*, 111–123. [CrossRef]